IEEE Photonics Journal
An IEEE Photonics Society Publication

Open Access

Experimental Demonstration of the Distributed Feedback Semiconductor Laser With S-Bent Waveguide and Sampled Grating

Volume 9, Number 5, October 2017

Yunshan Zhang
Yuechun Shi
Lianyan Li
Zhengpeng Zou
Jun Lu
Yinchao Du
Wenxuan Wang
Yating Zhou, *Member, IEEE*
Xin Chen
Jilin Zheng
Xiangfei Chen, *Senior Member, IEEE*

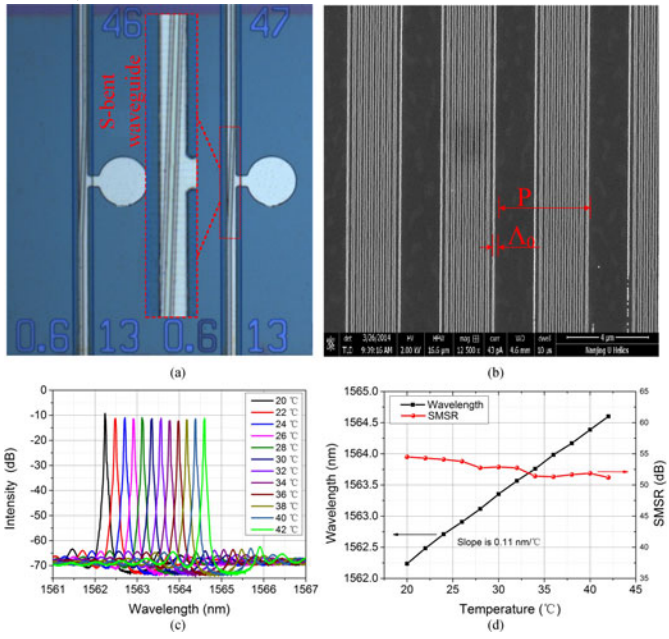

DOI: 10.1109/JPHOT.2017.2751573
1943-0655 © 2017 IEEE

Experimental Demonstration of the Distributed Feedback Semiconductor Laser With S-Bent Waveguide and Sampled Grating

Yunshan Zhang,[1,6] Yuechun Shi,[2] Lianyan Li,[1] Zhengpeng Zou,[2] Jun Lu,[2] Yinchao Du,[2] Wenxuan Wang,[2] Yating Zhou,[3] *Member, IEEE*, Xin Chen,[4] Jilin Zheng,[5] and Xiangfei Chen,[2] *Senior Member, IEEE*

[1]School of Optoelectronic Engineering, Nanjing University of Posts and Telecommunications, Nanjing 210023, China
[2]Microwave-Photonics Technology Laboratory, National Laboratory of Microstructures, and the School of Engineering and Applied Sciences, Nanjing University, Nanjing 210093, China
[3]School of Mathematics and Physics and Chemical Engineering, Changzhou Institute of Technology, Changzhou 213022, China
[4]Huagong Genuine Optics Co., Ltd., Wuhan 430223, China
[5]Photonics Information Technology Laboratory, Institute of Communication Engineering, PLA University of Science and Technology, Nanjing 210007, China
[6]Suzhou High-Tech Institute, Nanjing University, Suzhou 215123, China

DOI:10.1109/JPHOT.2017.2751573

Manuscript received July 21, 2017; revised August 29, 2017; accepted September 8, 2017. Date of publication September 12, 2017; date of current version September 29, 2017. This work was supported in part by the Natural Science Foundation for the Youth under Grants 61504058, 61504170, and 61405096, in part by the Nature Science Foundation of Jiangsu Province of China under Grants BK20141168, BK20140414, and BK20160907, in part by the National Nature Science Foundation of China under Grants 61640419, 61435014, 11574141, 61575186, and 61635001, in part by the National "863" project of China under Grant 2015AA016902, in part by the Scientific Research Foundation of the Nanjing University of Posts and Telecommunications under Grant 215041, in part by the Fundamental Research Funds for the Central Universities under Grant 021314380092. Corresponding author: Yating Zhou (e-mail: zhou-yating@163.com).

Abstract: A distributed feedback (DFB) semiconductor laser based on s-bent waveguide and sampled grating is theoretically studied and experimentally demonstrated. The proposed laser operates with a high side mode suppression ratio (SMSR) when the bias current is changed from 50 to 130 mA. When the bias current is fixed at 130 mA, the SMSR is larger than 55 dB, which is benefit from the suppressed spatial hole burning, while the SMSR of the equivalent phase shifted DFB laser decreases to 39 dB. The wavelength spacing error between two proposed DFB lasers is measured to be 0.089 nm compared with the designed value. When temperature is increased from 20 °C to 42 °C, the presented DFB laser achieves stable single longitudinal mode (SLM) operation with SMSR >51 dB and the wavelength varies from 1562.24 to 1564.6 nm with a slope of 0.11 nm/°C. The s-bent waveguide and sampled grating can be fabricated simply by the common holography exposure and photolithograph technique resulting in a low cost. Besides, the wavelength accuracy and SLM yield can be improved significantly, which is very beneficial for the multiwavelength DFB laser array.

Index Terms: DFB semiconductor laser, sampled grating, s-bent waveguide.

1. Introduction

DFB semiconductor lasers are the key element in the optical communications. Two key features are the single longitudinal mode (SLM) operation and the wavelength accuracy. Some methods have been proposed to improve the SLM yield of DFB lasers such as true phase shift and s-bent waveguide [1], [2]. To fabricate the DFB laser with true phase shift needs high procession precision [3], [4]. So the reconstruction equivalent chirp (REC) technique is invented by one of the authors of this paper to solve this problem [5]. To obtain the same performance, the procession precision for REC based DFB laser with equivalent phase shift (EPS-DFB laser) can be reduced one to two orders of magnitudes. With the development of the demand for the transmission capacity, multi-wavelength distributed feedback semiconductor laser arrays (DFB-MLAs) are considered as one of the most promising light source in the wavelength division multiplexing (WDM) networks and the photonic integrated circuits (PICs) [6]. In the future, it can be predicted that more and more channels (or wavelengths), as well as lasers will be integrated on the single chip [7], [8]. And then the lasing wavelength spacing between adjacent channels will become smaller and smaller. If the wavelength spacing is set to be 0.08 nm, even for fabricating the EPS-DFB laser array, the procession precision should be about 4.4 nm, which is high surprisingly.

On the other hand, either a DFB laser with true phase shift or an EPS-DFB laser, at large bias current the spatial hole burning (SHB) effect will degrade the side mode suppression ratio (SMSR) [9]–[11]. In order to overcome the problem of SMSR degradation, DFB lasers with complicated grating structures, e.g., the corrugation-pitch-modulated (CPM) grating, have been proposed [12], [13]. The most commonly used method to fabricate complicated gratings is the electron beam lithography (EBL) [14], [15]. It can accurately write the grating line by line to generate the complex grating patterns. However, it is time consuming as well as of high cost.

The DFB lasers with s-bent waveguide and sampled gratings designed by the REC technique have been theoretically studied in detail [16]. It predicts that DFB lasers with stable SLM and high wavelength accuracy can be achieved more simply by combining s-bent waveguide with the REC technique. The wavelength spacing precision can be also further improved employing the method mentioned in [16].

In this paper, we provide a proof-of-concept study on the DFB laser with s-bent waveguide and sampled gratings (SBW-DFB). The SBW-DFB laser is demonstrated experimentally. The proposed SBW-DFB laser has a stable SLM performance, e.g., under the temperature 25 °C the SMSRs are measured to be $>$47 dB when the bias current varies from 50 mA to 130 mA. When the bias current is fixed at 100 mA and the temperature is changed from 20 °C to 42 °C, the SBW-DFB laser can also achieve high stable SLM operation with SMSR $>$51 dB and the wavelength is changed from 1562.24 nm to 1564.6 nm with a slope of 0.11 nm/°C. Compared with the EPS- DFB laser, the SBW-DFB laser has higher SMSR and more stable SLM performance due to its weaker SHB effect. Two SBW-DFB lasers with wavelength spacing of 0.8 nm are designed and the measured wavelength spacing is 0.889 nm. That is to say, the deviation between the designed wavelength spacing and the measured value is only 0.089 nm. Utilizing the proposed method the wavelengths of the DFB lasers can be controlled with higher precision.

2. Device Design and Operating Principle

2.1 Device Operating Principle

The structure of the SBW-DFB laser is shown in Fig. 1(a). The SBW-DFB laser has the same semiconductor material with the conventional multiple-quantum-well (MQW) DFB laser. The grating in the SBW-DFB laser is a uniform sampled grating designed by the REC technique. The main difference between the EPS-DFB laser and the SBW-DFB laser is that there is an s-bent waveguide in the center of the SBW-DFB laser implementing a continuous phase change.

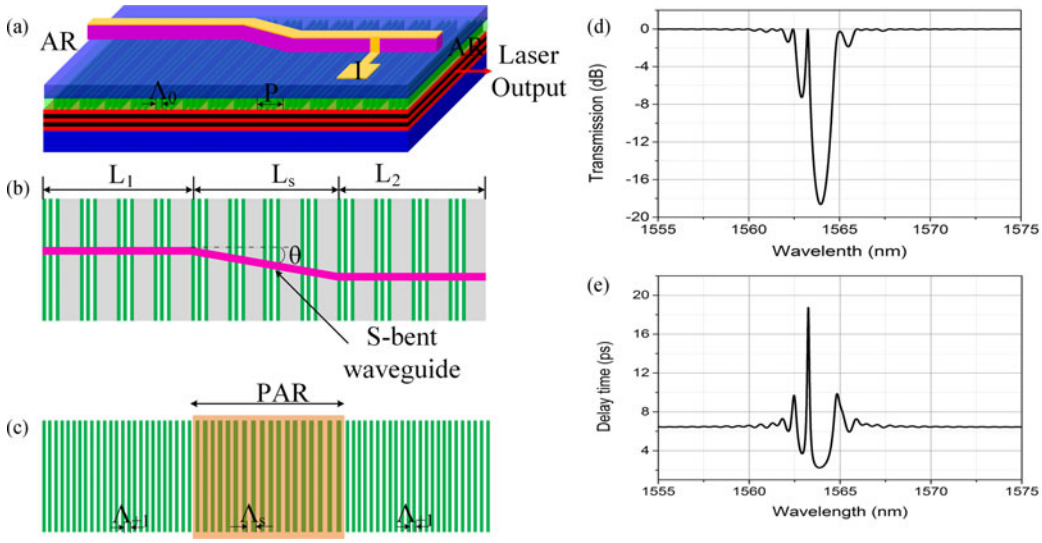

Fig. 1. Schematic of the (a) DFB laser with s-bent waveguide and sampled grating, (b) s-bent waveguide and sampled grating, (c) equivalent grating pattern in +1st subgrating, and (d) calculated transmission spectrum of a CPM grating, (e)calculated group delay of a CPM grating.

According to the Fourier analysis, the sampled grating as shown in Fig. 1(b) can be expressed as [17]

$$\Delta n\,(z) = \frac{1}{2}\Delta n_s \sum_m F_m \exp\left[j\left(2\pi\frac{z}{\Lambda_0} + 2m\pi\frac{z}{P}\right)\right] + c.c \tag{1}$$

where P is the sampling period, Λ_0 is the period of the seed grating, Δn_s is the index modulation of the seed grating, m denotes the mth order Fourier series and F_m is the Fourier coefficient of the mth subgrating. Usually the +1st order subgrating is used as the equivalent grating for DFB lasers, and the period of the +1st order subgrating Λ_{+1} can be expressed as

$$\Lambda_{+1} = \frac{\Lambda_0 P}{(P + \Lambda_0)} \tag{2}$$

Therefore, the lasing wavelength controlled by the +1st subgrating can be changed by tuning the sampling period P. The grating period in the bent waveguide region can be expressed as [16]

$$\Lambda_s = \frac{\Lambda_{+1}}{\cos\theta} = \frac{\Lambda_0 P}{(P + \Lambda_0)\cos\theta} \tag{3}$$

Here, θ is the tilted angle of the bent waveguide. The equivalent grating is shown in Fig. 1(c). It can be seen that Λ_s is larger than Λ_{+1}. And a continuous phase change can be induced in the bent waveguide region, which can be named as phase adjust region (PAR). Usually, a grating with PAR region also is called as corrugated pitch modulation (CPM) grating. Through changing the tilted angle θ of the bent waveguide, various phase shifts in the PAR can be realized. According to the [16], when a π phase shift is induced in the PAR, the relationship between Λ_s and Λ_{+1} should be expressed as follows:

$$\frac{L_s}{\Lambda_{+1}} - \frac{L_s}{\Lambda_s} = \frac{1}{2} \tag{4}$$

Fig. 1(d) and (e) show the calculated transmission spectrum and group delay time of a CPM grating with π phase shift. Compared with a normal π phase shift grating, it is obvious that the main mode of a CPM grating locates off the stop-band center of the transmission spectrum. As a consequence, the spectrum of the SBW-DFB laser will be asymmetric and the main mode will drift towards one side of the spectrum, which will be discussed in the following.

Table 1
Parameters of the SBW-DFB Lasers

Parameters	No. 1 SBW-DFB Laser	No. 2 SBW-DFB Laser	EPS-DFB laser
Total cavity length (μm)	600	600	600
L_1 (μm)	200	200	——
L_s (μm)	200	200	——
L_2 (μm)	200	200	——
Tilted angle θ	2°	2°	——
Seed grating period Λ_0 (nm)	258.189	258.189	258.189
Sampling period P (μm)	4.558	4.602	4.602
Effective refractive index (at 1550 nm)	3.2	3.2	3.2

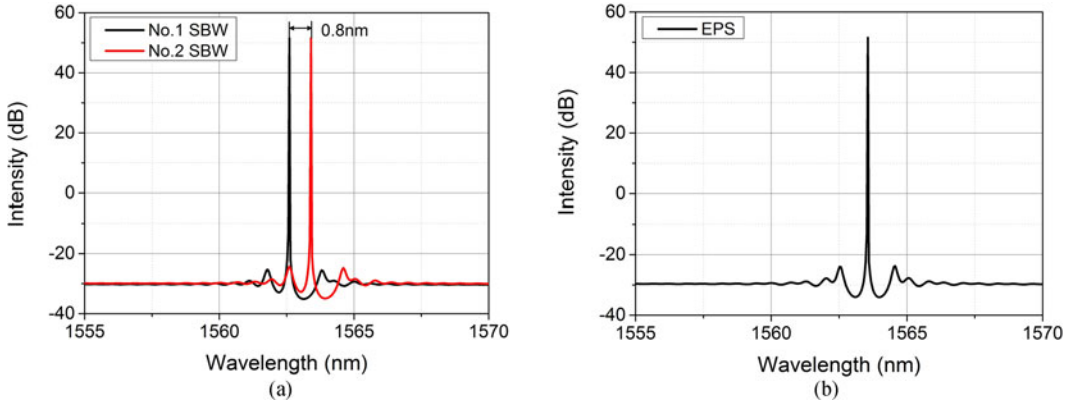

Fig. 2. Simulated spectra of the two types of DFB Lasers (a) with SBW structure, (b) with EPS structure.

2.2 Simulation Results

Utilizing the above mentioned structure, we have designed two SBW-DFB lasers with 0.8 nm wavelength spacing. The parameters of the two lasers are listed in Table 1. The total cavity length is 600 μm and the length of the s-bent area (L_s) is 200 μm with two 200 μm-long straight waveguides (L_1 and L_2) on both sides. The tilted angle of the s-bent waveguide is 2°. The Bragg wavelength of the seed grating is set at 1640 nm, which is far away from the gain region. In order to obtain 0.8 nm wavelength spacing, the sampling periods of the two DFB laser are designed as 4.558 μm and 4.602 μm respectively. For comparison, an EPS-DFB laser with straight waveguide and π EPS at the cavity center is also designed. The total cavity length and sampling period of the EPS-DFB laser are the same with the No. 2 SBW-DFB laser shown in Table 1.

We have simulated the characteristics of the two types of DFB lasers by the transfer matrix method (TMM) [18], [19]. Fig. 2(a) is the simulated spectra of the two SBW-DFB lasers. The simulated results indicate that both the SBW-DFB lasers operate in good SLM and the wavelength spacing between the two lasers is fixed at 0.8 nm exactly. We also can obtain the other wavelength spacing with different sampling periods. Then, MLA can be achieved in the single chip only by changing sampling period. Due to the equivalent CPM grating structure, the main modes of the SBW-DFB lasers are located off the stop-band center and the spectra are asymmetrical. However,

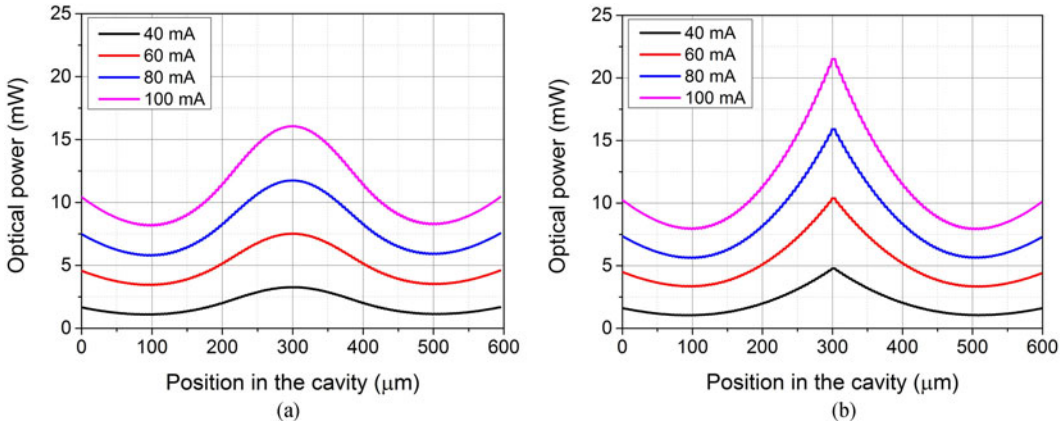

Fig. 3. Simulated light intensity distributions along the resonant cavity in (a) SBW-DFB laser, (b) EPS-DFB laser.

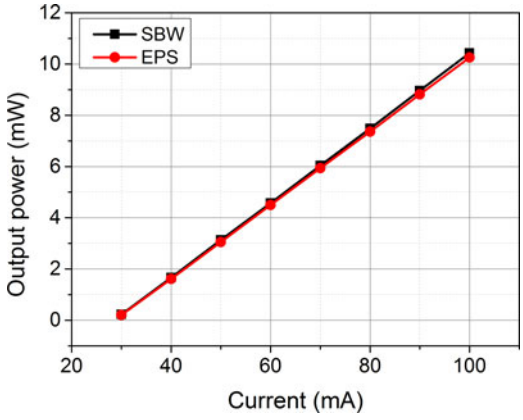

Fig. 4. Simulated P-I curve of the DFB lasers.

as shown in Fig. 2(b), the spectrum of the EPS-DFB laser is symmetrical and the main mode is located at the center of the stop-band.

The internal light intensity distributions along the resonant cavity at different bias currents are demonstrated in Fig. 3. Through comparing the Fig. 3(a) with Fig. 3(b), it can be seen that the internal light intensity distribution of the SBW-DFB laser is flatter than that of the EPS-DFB laser, i.e., weaker SHB effect in the SBW-DFB laser ensuring the better SLM property [20], [21].

Fig. 4 plots the calculated power–current (P–I) curves of the two types of DFB lasers. The simulated results indicate that the SBW-DFB laser and the EPS-DFB laser have the similar threshold and slope efficiency. The simulated thresholds of the SBW-DFB laser and EPS-DFB laser are about 28.5 mA and the slope efficiencies are 0.145 mW/mA and 0.14 mW/mA, respectively. The calculated slope efficiency of the SBW-DFB laser is a little higher than that of the EPS-DFB laser.

3. Experimental Results and Discussion

3.1 Experimental Results

The epi-wafer structure used for the device fabrication is similar to that of the common DFB laser. It is grown by a conventional two-stage metal-organic chemical vapor deposition (MOCVD). A n-InP buffer layer, a n-InAlGaAs lower optical confinement layer, an InAlGaAs MQW structure,

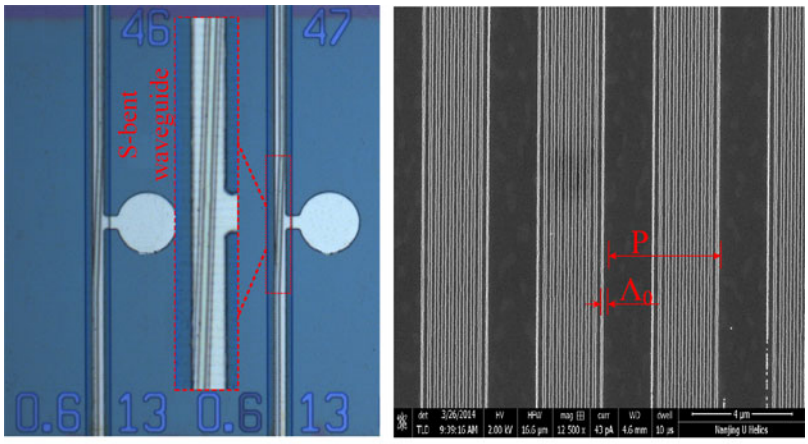

Fig. 5. (a) Photograph of the designed SBW-DFB lasers, inset is the enlarged photograph of the s-bent waveguide, (b) SEM image of the sampled grating.

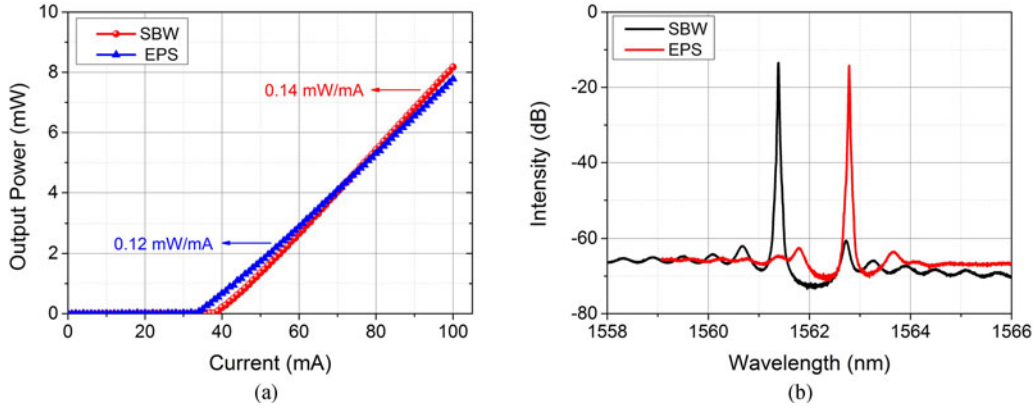

Fig. 6. The measured results of the fabricated DFB laser. (a) P-I curves and (b) spectra of the SBW-DFB laser and EPS-DFB laser.

a p-InAlGaAs upper optical confinement layer and a 30 nm thick p-InAlGaAs grating layer are successively grown on a n-InP substrate in the first epitaxial growth. The fabrication of the sampled grating is the same as the common method as shown in [17], [22]. The uniform sampled grating is firstly formed by a conventional holographic exposure combined with conventional photolithography. After the fabrication of the sampled grating, a p-InP cladding layer and a p-InGaAs contact layer are successively regrown over the entire structure. The devices are realized by processing s-bent ridge waveguides, opening p-metal contact windows, followed by metal contacts. Finally, antireflection coatings with reflectivity of less than 1% are applied to the both facets of devices.

The photograph of the fabricated DFB lasers is shown in Fig. 5(a) and the bent ridge waveguide can be observed clearly. Here, the bent angle is 2°. The scanning electron microscope (SEM) picture of the sampled grating is shown in Fig. 5(b). In addition, an EPS-DFB laser is also fabricated on the same wafer for comparison.

The P-I curves of the SBW-DFB laser and EPS-DFB laser are plotted in Fig. 6(a). The measured thresholds of the SBW-DFB laser and EPS-DFB laser are 37 mA and 35 mA, and the output slope efficiencies are 0.14 mW/mA and 0.12 mW/mA, respectively. The threshold of the SBW-DFB laser is a little larger than the EPS-DFB laser. But the SBW-DFB laser has higher output slope efficiency. The two differences are mainly caused by the s-bent waveguide. The one reason is that, because

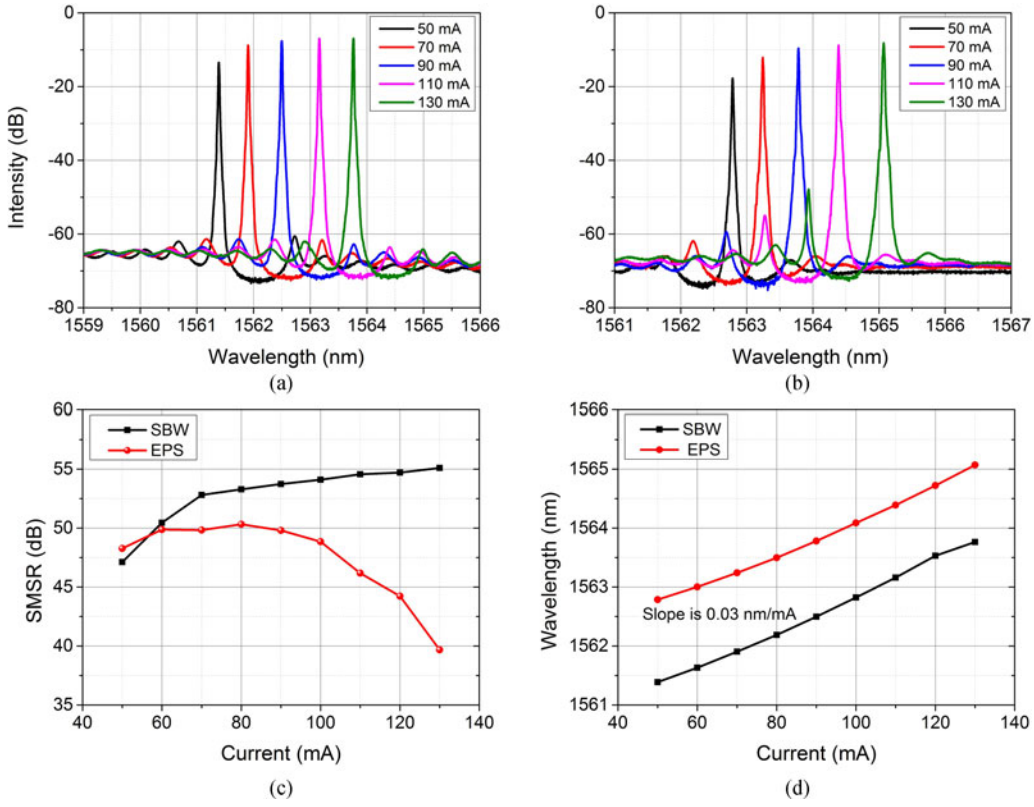

Fig. 7. The measured spectra of the fabricated laser under 25 °C and different bias currents with (a) the SBW-DFB laser and (b) the EPS-DFB laser. (c) The corresponding SMSRs with different bias currents and (d) the lasing wavelengths with different bias currents.

the resonance wavelength (i.e., transmission peak in Fig. 1(d) and (e)) blue shifts caused by the PAR grating region, the reflectivity of the grating is a little lowered, the threshold increases. But, on the other hand, the light penetration deep in longitudinal direction also increases, resulting in the high gain utilization and hence the high slope efficiency [2], [21]. The other reason is that the bent waveguide can lead to a little radiation loss. The measured spectra of the two DFB lasers with the same bias current are shown in Fig. 6(b). Both of the lasers achieve stable SLM operation. The spectrum of the SBW-DFB laser is asymmetric, which agrees well with the simulated result as shown in Fig. 2(a). At the same time, the spectrum of the EPS-DFB laser is nearly symmetric.

Fig. 7(a) and (b) show the spectra of the SBW-DFB laser and EPS-DFB laser at different bias currents both under the same temperature 25 °C. The SLM characteristics of the lasers at different bias currents are also measured. As shown in Fig. 7(a) and (c), when the bias current is changed from 50 mA to 130 mA, the SMSR of the SBW-DFB laser increases from 47 dB to 55 dB. By contrast, for the EPS-DFB laser once the bias current becomes larger than 80 mA (SMSR is 50 dB), the SMSR degenerates rapidly. When the bias current is 130 mA, the SMSR decreases to be 39 dB. A side mode in short wavelength side can be seen in Fig. 7(b), which is caused by the SHB effect [11]. While, thanks to the bent waveguide region in the SBW structure, SHB effect can be suppressed as shown in Fig. 3(a). Therefore, good SLM property can be maintained even at high injection current. Fig. 7(d) shows the wavelength shift versus the bias current. The two kinds of lasers have nearly the same wavelength shift ratio of 0.03 nm/mA.

Fig. 8 plots the P-I curves of the SBW-DFB laser at different temperatures. When the temperature is changed from 20 °C to 45 °C, the threshold rises from 39 mA to 49 mA and the slope efficiency is reduced from 0.14 mW/mA to 0.11 mW/mA.

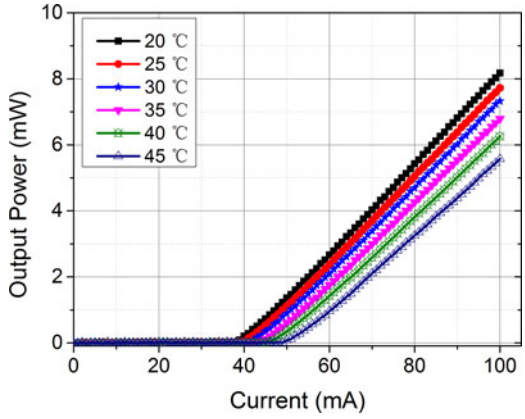

Fig. 8. P-I curves at different temperature.

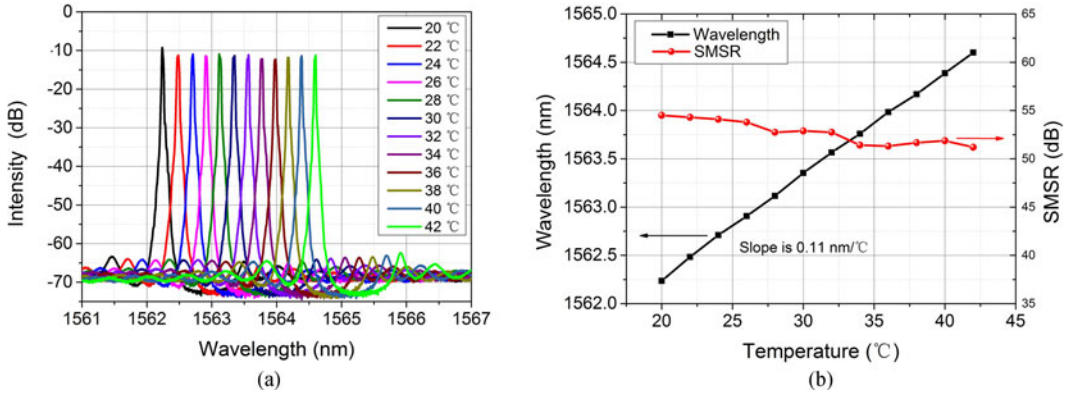

Fig. 9. (a) The measured spectra of the SBW-DFB laser at different temperatures, (b) the corresponding wavelengths and SMSRs of the SBW-DFB laser versus temperatures.

The spectra of the SBW-DFB laser with bias current of 100 mA under different temperatures are shown in Fig. 9(a). When the temperature rises from 20 °C to 42 °C, the SBW-DFB laser is in stable SLM state and the SMSR degenerates a little from 54.5 dB to 51.2 dB. The wavelength also drifts from 1562.24 nm to 1564.6 nm with a slope of 0.11 nm/°C.

One of the significant advantages of the proposed laser structure is that it can easily control the wavelength with high wavelength accuracy [16]. Fig. 10 shows the spectra of two SBW-DFB lasers which are fabricated adjacently on the same bar and measured at the same current of 100 mA. The sampling periods are 4.558 μm and 4.602 μm respectively as mentioned above for the designed wavelength spacing of 0.8 nm. All the other parameters are the same. The results indicate that both the two SBW-DFB lasers operate in good SLM with SMSRs higher than 52 dB and the wavelength spacing is 0.889 nm, which is 0.089 nm larger than the designed value showing good wavelength precision.

3.2 Discussion

The measured results indicate that the threshold of the proposed DFB laser, 37 mA, is a little higher than the EPS-DFB laser. This is caused by several reasons. First of all, the grating in the proposed DFB lasers is not strong enough and the coupling coefficient κ is measured to be only 20 cm^{-1}, i.e., the coupling coefficient-length product (κL) is 1.2. As shown in Fig. 11, we calculate the threshold of the SBW-DFB laser with various κL products utilizing the TMM method. The threshold current and

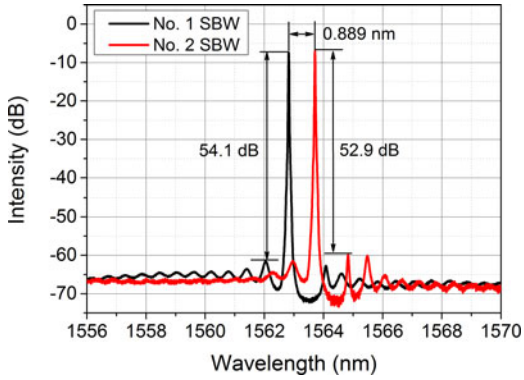

Fig. 10. The measured spectra of two SBW-DFB lasers at 100 mA bias current.

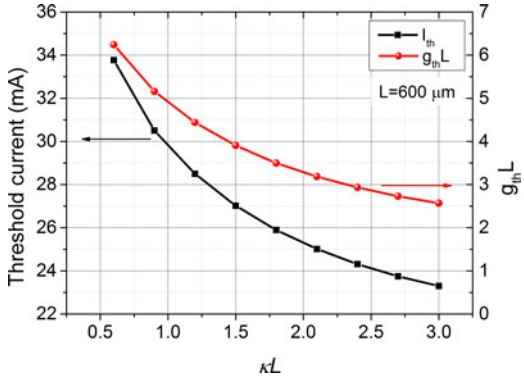

Fig. 11. The simulated threshold current and normalized threshold gain against κL.

normalized threshold gain (the threshold gain-length product gth L) with different κL products are plotted in Fig. 11. It can be inferred from the simulated results that the threshold can be decreased by employing stronger gratings with higher κL products. The grating in the proposed SBW-DFB laser is so weak, that the length of the cavity length should be lengthened to make sure that the DFB laser can operate normally. The cavity length of the SBW-DFB laser is 600 μm, which is about twice as long as that of a conventional DFB laser. So, in order to decrease the threshold of the SBW-DFB laser, we should enlarge the grating coupling coefficient κ and shorten the cavity length.

In this work, though the study mainly focuses on the single SBW-DFB laser, the results exhibit that the structure can be easily applied to the DFB-MLAs, which will be fabricated in the nearly future. According to the (2), the period of the $+1$st order subgrating Λ_{+1} varies with the sampling period *P*. So we can control the wavelength spacing of the REC based DFB-MLAs by adjusting the sampling period *P*. In the future, DFB-MLAs with wavelength spacing less than 0.1 nm is required [23]. However, it is difficult for the REC technique to obtain DFB-MLAs with so small wavelength spacing. For example, for the EPS-DFB laser studied in our manuscript, if the wavelength spacing is demanded to be 0.08 nm, the step change of *P* should be 4.43 nm. The required process precision is so high that it is very hard to obtain. According to the (3), for the SBW-DFB laser, the phase shift in the s-bent area can be adjusted by changing the tilted angle θ and then the lasing wavelength can be controlled. Fig. 12(a) shows the simulated spectra of 8-channel SBW-DFB-MLAs with wavelength spacing of 0.08 nm. As shown in Fig. 12(b), the small wavelength spacing is achieved by adjusting the tilted angle θ, in other words, by changing the transversal displacement H_s between the straight waveguides. In order to obtain wavelength spacing 0.08 nm in the No.2 SBW-DFB laser, that is, to change the lasing wavelength from 1563.12 nm to 1563.20 nm, the transversal displacement H_s

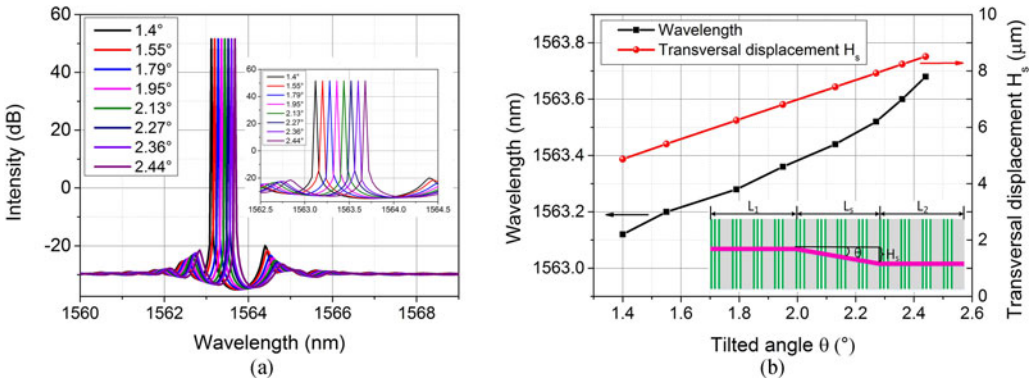

Fig. 12. (a)Simulated spectra of 8-channel SBW-DFB-MLA with 0.08 nm wavelength spacing, inset is the enlarged spectra, (b) the wavelength and transversal displacement H_s of the waveguide against the tilted angle, inset is the schematic of H_s.

should be changed from 4.87 μm to 5.41 μm. It can be concluded that to fabricate DFB-MLAs with the same wavelength spacing 0.08 nm, using EPS-DFB laser the demanded process precision is smaller than 1% of the one using SBW-DFB laser. It is obviously that the proposed method will greatly simplify the fabrication of DFB-MLAs with small wavelength spacing.

3. Conclusion

In this paper, a DFB laser based on s-bent waveguide and sampled grating is experimentally demonstrated. The DFB laser operates with high SMSR when the bias current and temperature are changed, i.e., high stable SLM performance is obtained. Additionally, the wavelength is controlled accurately utilizing the proposed method and the spectra agree well with the simulated results. The probability to achieve DFB-MLAs with much smaller wavelength spacing using the reported method is also discussed. Furthermore, the DFB lasers can be fabricated by the conventional holographic exposure and photolithography technique with much lower costs. The proposed method is a promising way to fabricate multichannel DFB laser arrays for photonic integrated circuits in the future.

References

[1] J. E. Whiteaway, G. Thompson, A. J. Collar, and C. J. Armistead, "The design assessment of λ/4 phase-shifted DFB laser structures," *IEEE J. Quantum Electron.*, vol. 25, no. 6, pp. 1261–1279, Jun. 1989.
[2] H. Hillmer, K. Magari, and Y. Suzuki, "Chirped gratings for DFB laser diodes using bent waveguides," *IEEE Photon. Technol. Lett.*, vol. 5, no. 1, pp. 10–12, Jan. 1993.
[3] T.-P. Lee *et al.*, "Multiwavelength DFB laser array transmitters for ONTC reconfigurable optical network test bed," *J. Lightw. Technol.*, vol. 14, no. 6, pp. 967–976, Jun. 1996.
[4] H. Zhu *et al.*, "The fabrication of eight-channel DFB laser array using sampled gratings," *IEEE Photon. Tech. Lett.*, vol. 22, no. 5, pp. 353–355, Mar. 2010.
[5] Y. Dai and X. Chen, "DFB semiconductor lasers based on reconstruction-equivalent-chirp technology," *Opt. Exp.*, vol. 15, no. 5, pp. 2348–2353, Mar. 2007.
[6] W. Li, X. Zhang, and J. Yao, "Experimental demonstration of a multi-wavelength distributed feedback semiconductor laser array with an equivalent chirped grating profile based on the equivalent chirp technology," *Opt. Exp.*, vol. 21, no. 17, pp. 19966–19971, Aug. 2013.
[7] S. Bao, Y. Xi, S. Zhao, and X. Li, "Sampled grating DFB laser array by periodic injection blocking," *IEEE J. Sel. Topics Quantum Electron.*, vol. 19, no. 5, pp. 1–8, Feb. 2013.
[8] T. L. Koch and U. Koren, "Semiconductor photonic integrated circuits," *IEEE J. Quantum Electron.*, vol. 27, no. 3, pp. 641–653, Mar. 1991.
[9] M. Okai, S. Tsuji, and N. Chinone, "Stability of the longitudinal mode inλ/4-shifted InGaAsP/InP DFB lasers," *J. Quantum Electron.*, vol. 25, no. 6, pp. 1314–1319, Jun. 1989.
[10] I. Orfanos, T. Sphicopoulos, A. Tsigopoulos, and C. Caroubalos, "A tractable above-threshold model for the design of DFB and phase-shifted DFB lasers," *IEEE J. Quantum Electron.*, vol. 27, no. 4, pp. 946–956, Apr. 1991.

[11] W. S. Rabinovich and B. J. Feldman, "Spatial hole burning effects in distributed feedback lasers," *IEEE J. Quantum Electron.*, vol. 25, no. 1, pp. 20–30, Jan. 1989.
[12] S. Ogita, Y. Kotaki, H. Ishikawa, and H. Imai, "Optimum design for multiple-phase-shift distributed feedback laser," *Electron. Lett.*, vol. 24, pp. 731–732, Jun. 1988.
[13] Y. Nakano, Y. Luo, and K. Tada, "Facet reflection independent single longitudinal mode oscillation of GaAlAs/GaAs DFB laser equipped with a gain-coupling mechanism," *Appl. Phys. Lett.*, vol. 55, pp. 1606–1608, Oct. 1989.
[14] T. Kjellberg, S. Nilsson, T. Klinga, B. Broberg, and R. Schatz, "Investigation on the spectral characteristics of DFB lasers with different grating configurations made by electron-beam lithography," *J. Lightw. Technol.*, vol. 11, no. 9, pp. 1405–1415, Sep. 1993.
[15] C. Vieu *et al.*, "Electron beam lithography: Resolution limits and applications," *Appl. Surf. Sci.*, vol. 164, no. 1/4, pp. 111–117, Aug. 2000.
[16] Y. C. Shi, R. Liu, S. C. Liu, and X. F. Chen, "A low-cost and high-wavelength-precision fabrication method for multi-wavelength DFB semiconductor laser array," *IEEE Photon. J.*, vol. 6, no. 3, Apr. 2014, Art. no. 2400112.
[17] J. Li *et al.*, "B experimental demonstration of distributed feedback semiconductor lasers based on reconstruction-equivalent-chirp technology," *Opt. Exp.*, vol. 17, no. 7, pp. 5240–5245, Mar. 2009.
[18] G. P. Agrawal and A. Bobeck, "Modeling of distributed feedback semiconductor lasers with axially-varying parameters," *IEEE J. Quantum Electron.*, vol. 24, no. 12, pp. 2407–2414, Dec. 1988.
[19] S. K. B. Lo and H. Ghafouri-Shiraz, "A method to determine the above-threshold stability of distributed feedback semiconductor laser diodes," *J. Lightw. Technol.*, vol. 13, no. 4, pp. 563–568, Apr. 1995.
[20] S. Ogita, Y. Kotaki, H. Ishikawa, and H. Imai, "Optimum design for multiple-phase-shift distributed feedback laser," *Electron. Lett.*, vol. 24, pp. 731–732, Jun. 1988.
[21] Y. Nakano, Y. Luo, and K. Tada, "Facet reflection independent single longitudinal mode oscillation of GaAlAs/GaAs DFB laser equipped with a gain-coupling mechanism," *Appl. Phys. Lett.*, vol. 55, pp. 1606–1608, Oct. 1989.
[22] Y. C. Shi *et al.*, "Experimental demonstration of eight-wavelength distributed feedback semiconductor laser array using equivalent phase shift," *Opt. Lett.*, vol. 37, no. 16, pp. 3315–3317, Aug. 2012.
[23] M. Presi, R. Corsini, M. Artiglia, and E. Ciaramella1, "Ultra-dense WDM-PON 6.25 GHz spaced 8x1 Gb/s based on a simplified coherent-detection scheme," *Opt. Exp.*, vol. 23, no. 17, pp. 22706–22713, Aug. 2015.